Study of Rotor Tip-Clearance Flow Using Large-Eddy Simulation

Donghyun You,* Meng Wang,† Rajat Mittal,‡ and Parviz Moin§

*†§ *Stanford University, Stanford, CA 94305*
‡ *The George Washington University, Washington, DC 20052*

Abstract

A large-eddy simulation has been performed to study the temporal and spatial dynamics of a rotor tip-clearance flow, with the objective of determining the underlying mechanisms for low pressure fluctuations downstream of the tip-gap. Simulation results are compared with experimental measurements, and favorable agreements are observed in both qualitative and quantitative sense. Typical vortical structures such as the tip-leakage vortex and tip-separation vortices are revealed, and their evolution is shown to be strongly influenced by the moving endwall and the blade wake. These vortical structures are the main sources of turbulence energy and Reynolds stresses as well as low-pressure fluctuations. Cavitation-inception analysis shows a high correlation between cavitation and the tip-leakage vortex.

Introduction

In hydraulic turbomachines, the existence of tip-clearance is a major source of cavitation, acoustic noise and performance deterioration. It is generally recognized that cavitation is associated with low-pressure fluctuations downstream of the rotor tip-gap (the region between the rotor-tip and the casing wall). To understand the mechanisms for the low pressure fluctuations, it is necessary to study the detailed turbulence dynamics in the rotor-blade wake and the tip-clearance region.

Previous experimental studies[1−5] have revealed various qualitative and some quantitative features of the tip-clearance flow. In the recent experiments performed by Devenport's group at Virginia Tech, Muthanna[4] and Wang[5] made detailed measurements of the flow field downstream of rotor blades in a low-speed linear compressor cascade employing stationary and moving endwalls to study the effects of the relative motion between the rotor blade-tip and the casing.

These experiments have provided useful information about the flow as well as valuable data for validating computational techniques. However, significant gaps still exist in our knowledge about the detailed dynamics of the tip-clearance flow and the resulting cavitation-inducing low-pressure events. This is primarily due to the difficulty in making detailed measurements in moving blade or endwall casing as well as simultaneously measuring velocity, vorticity and pressure. The flow phenomena of interest involve complex interactions among the tip-leakage vortex, tip-separation vortex, blade boundary-layer and wake, and the turbulent endwall boundary-layer. From a computational standpoint, given the highly unsteady nature of the flow and the need to resolve a range of important flow scales, it is beyond the capability of the Reynolds-averaged Navier-Stokes (RANS) approach.

As an alternative, we performed a large-eddy simulation (LES) of rotor tip-clearance flow using a newly developed solver which combines an immersed boundary technique with a curvilinear structured grid.[6] LES is better suited for studying such unsteady flows since it has the capability of resolving the energy containing scales temporally as well as spatially. The relatively low Reynolds numbers ($Re = O(10^5)$) encountered in typical turbomachinery configurations coupled with physically reasonable simplifications in the geometry, as well as access to high performance parallel computer systems, make these flows within the reach of LES.

A highly accurate LES of this flow is nonetheless very challenging due to the large mesh-size requirement, the fully three-dimensional nature of the simulation, and the need for statistical convergence and long-time sampling. In an initial attempt, a relatively "coarse" grid with approximately 7.9 million grid points was used, and results were presented in Ref. 6. Compared with the experimental findings[5] the tip-leakage vortex predicted by the coarse grid LES was smaller in size and its location was shifted. A careful analysis indicated that this was due to insufficient grid resolution, which was particularly severe in the streamwise direction. The poor resolution caused a delayed initiation of the tip-leakage vortex and its premature breakdown in the downstream direction. The tip-separation vortices were not clearly identified. The resolution issue was also reflected in the predicted energy spectra which dropped off too rapidly at higher frequencies.[6]

In the present study, we perform an LES with a

---

*Graduate Research Assistant, Center for Turbulence Research. Student Member AIAA

†Senior Research Scientist, Center for Turbulence Research. Member AIAA

‡Associate Professor, Department of Mechanical and Aerospace Engineering. Member AIAA

§The Franklin P. and Caroline M. Johnson Professor of Engineering; Director of Center for Turbulence Research. Associate Fellow AIAA

refined mesh estimated from the previous coarse-mesh simulation.[6] The grid size is increased to approximately 20.3 million grid points, with a simultaneous reduction in the streamwise domain size. This combination results in a resolution refinement of over 3.5 times. The same flow configuration as in the experimental setup of Devenport's group at Virginia Tech.,[4,5] involving a linear cascade with tip-clearance and moving endwall, is considered.

In what follows, a brief summary of the numerical techniques developed for the tip-gap flow and the flow configuration will be given first, followed by qualitative and quantitative comparisons of the velocity fields from the present LES and experiments.[4,5] The detailed vortex and flow dynamics will also be discussed. Finally, a preliminary analysis of low-pressure fluctuations and cavitation inception will be presented.

Simulation Methodology

A. Numerical Method

The numerical algorithm is based upon the generalized-coordinate Navier-Stokes solver of Choi *et al.*,[7] with significant enhancements to treat the special difficulties associated with the tip-clearance flow as described in Ref. 6. The spatially filtered Navier-Stokes equations for resolved scales in LES are as follows:

$$\frac{\partial \bar{u}_i}{\partial t} + \frac{\partial}{\partial x_j}\bar{u}_i\bar{u}_j = -\frac{\partial \bar{p}}{\partial x_i} + \frac{1}{Re}\frac{\partial}{\partial x_j}\frac{\partial \bar{u}_i}{\partial x_j} - \frac{\partial \tau_{ij}}{\partial x_j}, \quad (1)$$

$$\frac{\partial \bar{u}_i}{\partial x_i} = 0, \quad (2)$$

where τ_{ij} is the subgrid scale (SGS) stress tensor. All the coordinate variables, velocity components, and pressure are nondimensionalized by the total chord C, the free-stream velocity u_∞, and ρu_∞^2, respectively. The time is normalized by C/u_∞. The governing equations (1) and (2) are discretized in a conservative form in generalized coordinates using a staggered grid. The terms in the transformed equations are described in detail in Ref. 7.

The SGS stress tensor τ_{ij} is modeled by a Smagorinsky type eddy-viscosity model. Given the fully inhomogeneous nature of the flow, it is necessary to implement a Lagrangian dynamic SGS model[8] which averages the model coefficient along the flow pathlines as opposed to the homogeneous flow direction in the standard dynamic model.[9]

The difficulty with grid topology in the tip-clearance region is overcome by a novel approach which combines an immersed boundary technique[10] with a structured grid in generalized coordinate system. In addition to this, the high stagger angle in the experimental setup necessitates the use of very skewed mesh (cf. Figs. 1–3), which requires fine control of mesh parameters such as stretching ratio and aspect ratio, and an adequate formulation of nonlinear convection terms

to avoid numerical instability. Extensive studies revealed that the divergence form and skew-symmetric form lead to superior stability characteristics as compared to the rotational form.[6] More details on the grid topology and grid skewness issue are given in Ref. 6.

The integration method used to solve the transformed governing equations is based on a fully-implicit fractional-step method which avoids the severe time-step restriction in the tip-clearance region. All terms including cross-derivative diffusion terms are advanced in time using the Crank-Nicolson method and are discretized in space by second-order central-differencing. The numerical scheme is energy-conserving and more suitable for turbulent flow simulations than higher-order upwind schemes.[11] A Newton iterative method is used to solve the discretized nonlinear equations.

For the pressure Poisson equation, an efficient multigrid procedure, which is a combination of the Gauss-Seidel multigrid method in two-directions and a tridiagonal solver in the other direction, is used. This method is particularly appropriate for parallelization. Since the Poisson solver is the most expensive part of computation in this fully three-dimensional flow, it is crucial to improve both the convergence ratio and the parallel efficiency.

The simulation code is parallelized using OpenMP for shared-memory parallel computers. A difficulty encountered with the large mesh-size simulation is the stack memory requirement which exceeds the available amount on certain computer systems. Therefore, remedies such as dynamic memory allocation/deallocation and stackable array splitting have been implemented to make the simulation feasible with minimum loss in parallel efficiency.

B. Flow Configuration

The flow configuration and coordinate definition are schematically shown in Fig. 1. The present study is focused on a linear cascade matching the experimental setup of Wang.[5] The rotor blade has a small tip-clearance with the endwall as shown in Fig. 2(a). The computational domain is of size $L_x \times L_y \times L_z = 1.6C \times 0.929C \times 0.5C$. The full domain and grid distribution in a plane perpendicular to the blade (parallel to the endwall) is shown in Fig. 2(b). The third direction is Cartesian with non-uniform grid distribution (see Fig. 2(a)). The rotor is placed near the inflow station so as to leave an adequate region for analysis of downstream turbulence. The simulation is performed in a frame of reference attached to the rotor, with a moving endwall at the bottom of the tip-gap. This is consistent with the experiment of Wang,[5] where a moving belt is used as the endwall. Periodic boundary conditions used in the y-direction allow us to mimic the flow in the interior of a cascade. A simplification is made by terminating the blade-span to one-half chord length and imposing inviscid flow boundary conditions on that boundary:

$$\frac{\partial u}{\partial z} = \frac{\partial v}{\partial z} = w = 0 \quad \text{at} \quad z = 0.5C. \quad (3)$$

This can be justified by observing that the root vortex

at the hub does not play any significant role in the convected low pressure fluctuations which are found near the endwall. In Wang's experiment,[5] the tip-leakage vortex extends to about one-quarter of a chord length from the endwall. The inflow turbulent boundary-layer data are provided using the method of Lund *et al.*,[12] modified to account for the fact that the mean flow direction is not perpendicular to the inflow/outflow plane. No-slip boundary conditions are applied along the rotor blade and moving endwall:

$$u = w = 0, \quad v = V_{belt} \quad \text{at} \quad z = 0, \qquad (4)$$

and the convective boundary condition,

$$\frac{\partial u_i}{\partial t} + U_c \frac{\partial u_i}{\partial x_1} = 0, \qquad (5)$$

is applied at the exit boundary, where the convection speed U_c is set equal to the mean streamwise velocity integrated across the exit plane.

The other important simulation parameters are as follows: The size of the tip-clearance is 1.6% of the total chord, blade pitch is 0.9 chord, and the blade span is 0.5 chord (1 chord in the experiments[4,5]). The blade has a relatively high stagger-angle of about 57 degrees (see Fig. 2(b)). The Reynolds number of this flow is 400,000 based on the chord and inflow free-stream velocity, and the inflow turbulent boundary layer has a Reynolds number of 780 based on the momentum thickness.

Results and Discussion

A. Flow Field

The mesh size used for the present simulation is $449 \times 351 \times 129$ ($x \times y \times z$), which is about 2.6 times the size of the previous grid[6] ($321 \times 256 \times 96$). Meanwhile, the streamwise domain size has been reduced from $4C$ in the previous simulation to $1.6C$. The combination of the above two factors results in a grid refinement of more than 3.5 times in the streamwise direction. Various diagnostics for the mesh quality such as stretching ratio, mesh aspect ratio and smoothness have been carried out in the construction of the final mesh. As will be demonstrated, the current results are indeed much improved over the coarse-mesh solutions presented in Ref. 6.

Comparisons of the flow fields have been made between the present LES solutions and experimental measurements[4,5] in the downstream locations as shown in Fig. 3. In the experiments, four sets of hot wire measurements were taken to obtain detailed information of the mean and turbulent flow fields downstream of the compressor cascade, in planes 1 and 2 shown in the figure.

Figure 4 shows contour plots of the mean streamwise velocity at several locations along the span of the rotor blade ($z/C_a = 0.0018$, 0.183, 0.366, and 0.641). Here C_a is the axial chord length by which the locations are normalized. Away from the tip-gap region the flow is nearly two-dimensional in the statistical sense. In the first plane near the bottom, the contour lines show traces of the tip-leakage vortex and the counter-rotating passage vortex in the endwall region. Flow separation is observed on the suction side of the blade near the trailing edge. The tip-leakage vortex and the blade wake convects downstream with an angle.

The mean streamwise velocity from the LES is compared with experimental values in Figs. 5 and 6, at two downstream measurement locations $x/C_a = 1.51$ and $x/C_a = 2.74$, respectively, as seen by an observer looking upstream. Vertical bundles of the mean streamwise velocity contours are present in the wakes of rotor blades, and the tip-leakage vortices are found near the endwall in both the simulation and the experiment.[5] Compared with the experimental findings, agreements are generally good, and remarkably better in both the vortex size and location than in the previous coarse mesh LES.[6] This confirms our conjecture that the streamwise resolution is crucial for the adequate evolution of vortical structures in the tip-leakage flow. Note that the velocities shown in Figs. 5, 6, and 8 are normalized by the local maximum velocity in the plane to account for the mass leakage in the experiments. A recently published RANS simulation of this configuration in the stationary endwall case[13] also indicated an under-estimation of velocity magnitude in the experiment.[4]

The refined grid-resolution has not only improved the tip-leakage vortex size and strength, but also its downstream position. This effect is demonstrated in Fig. 7, which shows the mean spanwise velocity in an x-y plane. Three-distinct vortical structures are seen starting in the tip-gap region and extending downstream at an angle with the suction surface. The main feature in the middle is the tip-leakage vortex, the one slightly upstream is the counter-rotating passage vortex, and the remaining small structures are related to the tip-separation vortices. Compared to those from the coarse-mesh LES (Fig. 7(a)), the origins of the vortical structures have moved upstream (Fig. 7(b)), resulting in a shift in their downstream positions and better agreement with the experiment. Past experience[14] has shown that inadequate streamwise resolution leads to excess streamwise momentum in turbulent boundary-layers making them more resistant to separation. It appears that increasing the streamwise resolution of the attached blade boundary layer has led to earlier separation both from the blade surface and the tip region.

In Fig. 8 the wake profiles downstream of the rotor, obtained at $z/C_a = 0.9$ in the present LES and $z/C_a = 1$ in the experiment with a stationary endwall,[4] are plotted. The LES is seen to capture the correct location of the wake in all the measurement planes, although discrepancies in the profiles, particularly on the pressure side, are observed. The somewhat wider wake is also observed in the contour plots in Figs. 5 and 6. These discrepancies, and the remaining inconsistency in the size of tip-leakage vortex shown in Figs. 5 and 6, are likely caused by the insufficient domain size and resolution in the spanwise (z) direction as well as the

mass leakage in experiment.

The tip-leakage flow and the blade wake are the main sources of turbulent fluctuations and energy. Reynolds stresses are compared with the experimental data[5] in Figs. 9–11. They show reasonable agreements. The energy spectra from the present LES, coarse-mesh LES,[6] and the experiment[5] in the tip-leakage region ($x/C_a = 1.51$, $y/C_a = 1.8$, $z/C_a = 0.1$) are shown in Fig. 12. The spectra from both the LES and the experiment show presence of the inertial subrange. The numerical scheme is capable of predicting the energies in a wide range of frequencies without excessive numerical dissipation. The present LES shows improved results in the higher frequency range compared with the previous coarse-mesh LES.[6]

Figures 9–12 indicate that the tip-leakage vortex plays a dominant role in the generation of turbulence, and hence intense pressure fluctuations, in the downstream flow-field near the endwall region. To better identify the vortical structures, the λ_2 vortex identification method[15] is used. Figure 13 shows typical vortical structures predicted by the present LES as visualized by the λ_2 iso-surfaces. The most dominant vortical structure is the tip-leakage vortex which is generated near the leading-edge and convects downstream expanding the size (A in Fig. 13(a)). This is accompanied by counter-rotating vortical structures B, which are generated further upstream and terminated in the blade passage by the blocking effect of the neighboring blade. Small vortical structures abundant near the trailing-edge region (C in Fig. 13(a)) are related to the tip-separation vortices. They are extremely complicated due to interaction with the tip-leakage vortex from the neighboring blade. Similar observations have been reported by experiments.[4,5]

As seen in Fig. 13(b), as a result of interacting with the tip-separation vortices near the trailing-edge of a neighbor blade, the tip-leakage vortex becomes more complicated and evolves into a bunch of small scale vortical structures. This observation could explain the peak low pressure events in the downstream endwall region. Figure 14 shows the time history of pressure fluctuations in the downstream tip-leakage region at $x/C_a = 1.51$, $y/C_a = 1.8$, $z/C_a = 0.1$. This result indicates that the tip-leakage vortex is observed in the downstream endwall as a continuous passing of discrete vortical structures.

B. Low-Pressure Fluctuations

Detailed statistics of negative pressure fluctuations are being collected and analyzed in order to study cavitation. Figure 15 shows an example of the instantaneous (Fig. 15(a)), time-averaged (Fig. 15(b)) and root-mean squared (Fig. 15(c)) pressure contours in an x-y plane inside of tip-gap. The spatial and temporal variations of the negative pressure relative to the mean values appear to be highly correlated with the vortical structures in the tip-leakage flow, particularly in the tip-leakage and tip-separation vortices.

The negative pressure regions are susceptible to cavitation. Figure 16 shows an example of cavitation inception analysis using the minimum tension criterion proposed by Joseph.[16] This criterion is based on the normal stress of the fluid and the critical vapor pressure:

$$B_{ii} \doteq \tilde{\tau}_{ii} - p + p_c > 0, \qquad (6)$$

where $\tilde{\tau}_{ii}$ is the normal stress, p is local pressure and p_c is the pressure in the cavity. For this example, p_c of 0.01 is used, assuming the cavitation number of 0.02 based on the cascade inlet pressure. If all three components of the stress B_{11}, B_{22} and B_{33} are positive, a cavity will open. Similar discussions can be found in Knapp $et\ al.$[17]

Instantaneous and time-averaged contours of $B = 1/3(B_{11} + B_{22} + B_{33})$ are plotted in Figs. 16(a) and 16(b), respectively, in regions where all three components are positive. High levels of B in both the instantaneous and time-averaged contours are again concentrated in the tip-leakage region. In particular, the tip-leakage vortex appears as the dominant source of cavitation, and the tip-separation vortex is less important in comparison even though it involves equally low pressure (cf. Fig. 15). This is due to the high positive values of the normal stress $\tilde{\tau}_{ii}$ found in the tip-leakage vortex.

Conclusions

A large-eddy simulation has been performed to study the temporal and spatial dynamics of a rotor tip-clearance flow, with the objective of determining the underlying mechanisms for low pressure fluctuations which can lead to cavitation.

The simulation results show favorable agreements with experimental data in qualitative and quantitative comparisons. They also demonstrate marked improvement over the previous simulation using a coarser grid, indicating that mesh-resolution is critical to an accurate description of the complex vortex dynamics. Typical vortical structures including the tip-leakage vortex and tip-separation vortices are revealed using a vortex identification method. Their evolution is strongly affected by the moving endwall and blade-wake, inducing complicated dynamics of the vortical structures.

The tip-leakage vortex, tip-separation vortex, and blade-wake appear as the main sources of turbulence energy, Reynolds stresses, as well as low-pressure fluctuations. Strong pressure fluctuations which may be responsible for cavitation and acoustic noise have also been observed. An analysis based on low-pressure fluctuations and normal stress of the flow shows that cavitation inception has a high correlation with the prominent vortical structures in the tip-clearance configuration, particularly the tip-leakage vortex.

Acknowledgments

References

[1]Wenger, C. W., Devenport, W. J., Wittmer, K. S., and Muthanna, C., "Two-Point Measurements in the Wake of a Compressor Cascade," *AIAA 98-2556*.

[2]Kameier, F., and Neise, W., "Experimental Study of Tip Clearance Losses and Noise in Axial Turbomachines and Their Reduction," *Journal of Turbomachinery*, Vol. 119, 1997, pp. 460-471.

[3]Zierke, W. C., Farrel, K. J., and Straka, W. A., "Measurement of the Tip Clearance Flow for a High-Reynolds-Number Axial-Flow Rotor," *Journal of Turbomachinery*, Vol. 119, 1995, pp. 1-8.

[4]Wang, Y., "Tip Leakage Flow Downstream of a Compressor Cascade with Moving End Wall," Master Thesis, Department of Aerospace Engineering, Virginia Polytechnic Institute and State University, Feb., 2000.

[5]Muthanna, C., "Flowfield Downstream of a Compressor Cascade with Tip Leakage," Master Thesis, Department of Aerospace Engineering, Virginia Polytechnic Institute and State University, Feb., 1998.

[6]You, D., Mittal, R., Wang, M., and Moin, P., "Large-Eddy Simulation of a Rotor Tip-Clearance Flow," *AIAA 2002-0981*.

[7]Choi, H., Moin, P., and Kim, J., "Turbulent Drag Reduction: Studies of Feedback Control and Flow over Riblets," Report TF-55, Department of Mechanical Engineering, Stanford University, Stanford, CA, Sept., 1992.

[8]Meneveau, C., Lund, T. S., and Cabot, W. H., "A Lagrangian Dynamic Subgrid-Scale Model of Turbulence," *Journal of Fluid Mechanics*, Vol. 319, 1996, pp. 233-242.

[9]Germano, M., Piomelli, U., Moin, P., and Cabot, W. H., "A Dynamic Subgrid-Scale Eddy-Viscosity Model," *Physics of Fluids*, Vol. A 3, 1991, pp. 1760-1765.

[10]Fadlun, E. A., Verzicco, R., Orlandi, P., and Mohd-Yusof, J., "Combined Immersed-Boundary Finite-Difference Methods for Three-Dimensional Complex Flow Simulations," *Journal of Computational Physics*, Vol. 161, 2000, pp. 35-60.

[11]Mittal, R., and Moin, P., "Suitability of Upwind-Biased Schemes for Large-Eddy Simulation of Turbulent Flows," *AIAA Journal*, Vol. 36, No. 8, 1997, pp. 1415-1417.

[12]Lund, T. S., Wu, X., and Squires, K. D., "Generation of Turbulent Inflow Data for Spatially-Developing Boundary Layer Simulations," *Journal of Computational Physics*, Vol. 140, 1998, pp. 233-258.

[13]Khorrami, M. R., Li, F., and Choudhan, M., "Novel Approach for Reducing Rotor Tip-Clearance-Induced Noise in Turbofan Engines," *AIAA Journal*, Vol. 40, 2002, pp. 1518-1528.

[14]Kaltenbach, H.-J., Fatica, M., Mittal, R., Lund, T. S., and Moin, P., "Study of Flow in a Planar Asymmetric Diffuser Using Large-Eddy Simulation," *Journal of Fluid Mechanics*, Vol. 390, 1999, pp. 151-185.

[15]Jeong, J., and Hussain, F., "On the Identification of a Vortex," *Journal of Fluid Mechanics*, Vol. 285, 1995, pp. 69-94.

[16]Joseph, D. D., "Cavitation and the State of Stress in a Flowing Liquid," *Journal of Fluid Mechanics*, Vol. 366, 1998, pp. 367-378.

[17]Knapp, R. T., Daily, J. W., and Hammitt, F. G., *Cavitation*, McGraw-Hill, 1970.
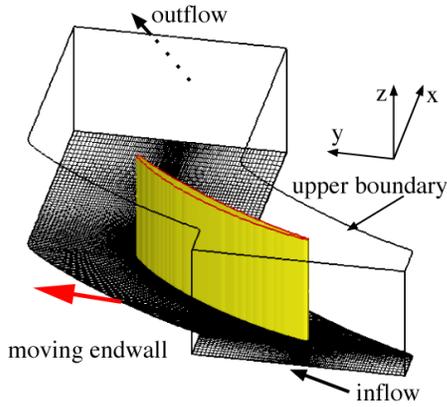
Figure 1: Flow configuration and coordinate system for LES of rotor tip-clearance flow.
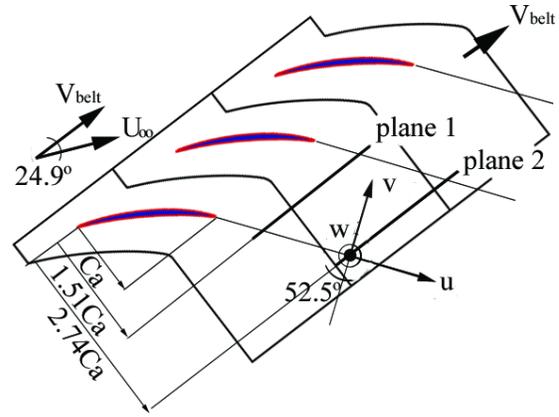
Figure 3: Measurement planes where comparisons are made between present LES and experiment.[5]

(a)

(b)
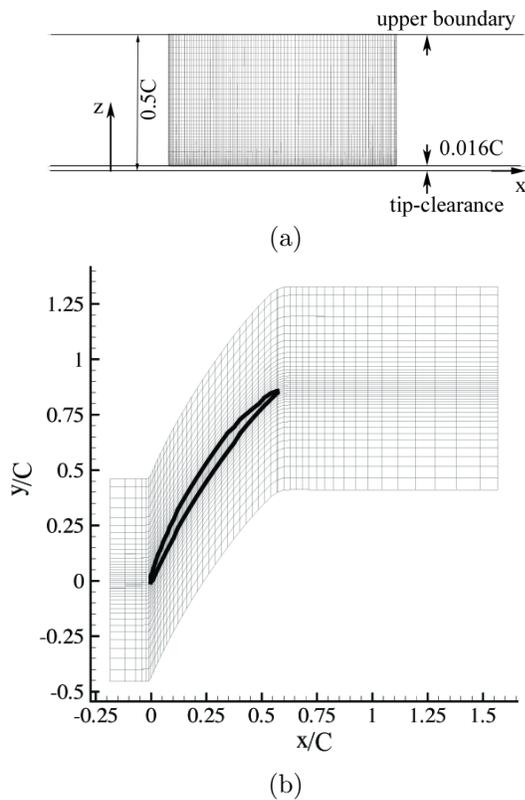
Figure 2: Computational domain for tip-clearance flow. (a) Cartesian mesh distribution on the blade in the $z-$direction (1/2 lines plotted); (b) curvilinear mesh in the $x-y$ plane used in conjunction with immersed boundary method (1/6 lines plotted).
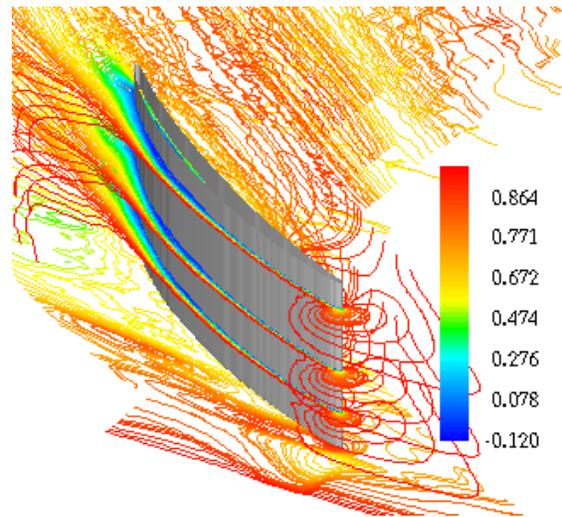
Figure 4: Contour plots of mean streamwise velocity at $z/Ca = 0.0018$, 0.183, 0.366 and 0.641. Contour levels are from -0.12 to 0.87 by 0.02.

(a)   (b)
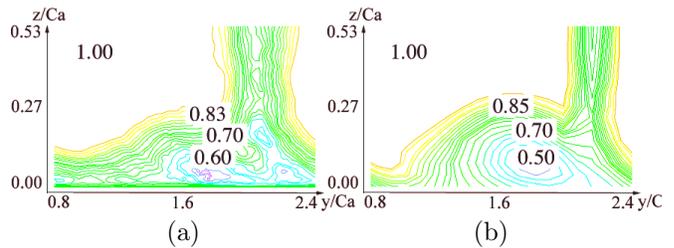
Figure 5: Comparison of mean streamwise velocity normalized by the local maximum velocity at $x/Ca = 1.51$. (a) present LES; (b) experiment.[5] Contour levels are from 0.5 to 1.0 by 0.025.

(a)

(b)
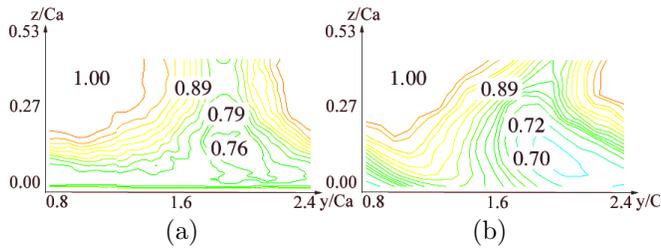
Figure 6: Comparison of mean streamwise velocity normalized by the local maximum velocity at $x/Ca = 2.74$. (a) present LES; (b) experiment.[5] Contour levels are from 0.5 to 1.0 by 0.025.

(a)

(b)

Figure 9: Comparison of Reynolds stress $\overline{u'u'}$ at $x/Ca = 1.51$. (a) present LES; (b) experiment.[5] Contour levels are from 0.003 to 0.012 by 0.0004.

(a)

(b)

Figure 7: Contour plots of mean spanwise velocity at $z/Ca = 0.008$. (a) coarse mesh LES[4]; (b) present LES. Contour levels are from -0.06 to 0.06 by 0.005.

(a)

(b)
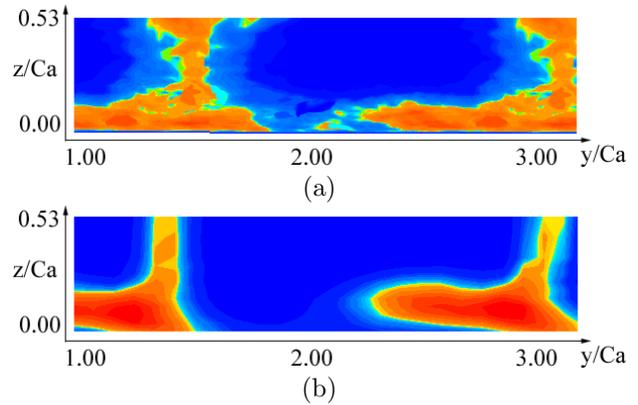
Figure 10: Comparison of Reynolds stress $\overline{v'v'}$ at $x/Ca = 1.51$. (a) present LES; (b) experiment.[5] Contour levels are from 0.003 to 0.012 by 0.0004.

Figure 8: Mean streamwise velocity profiles in the rotor-blade wake. Lines are from the present LES, and symbols are from the experiment.[4] Solid line and circle, $x/Ca = 1.366$; dashed line and square, $x/Ca = 2.062$; dotted line and triangle, $x/Ca = 2.74$.

(a)

(b)
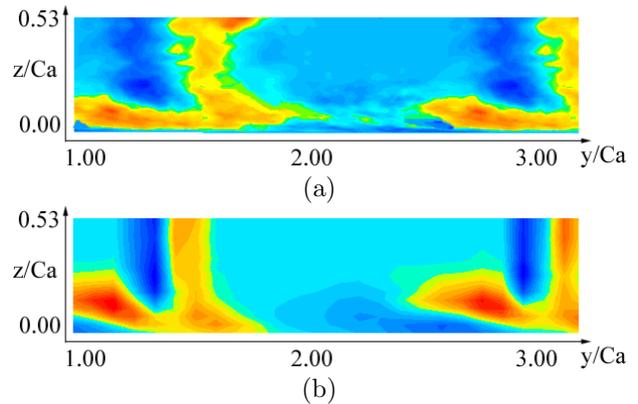
Figure 11: Comparison of Reynolds stress $\overline{u'v'}$ at $x/Ca = 1.51$. (a) present LES; (b) experiment.[5] Contour levels are from -0.004 to 0.004 by 0.0004.
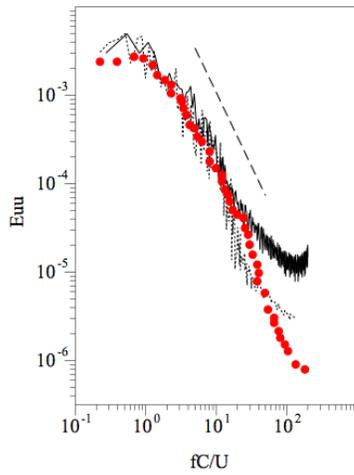
(a)
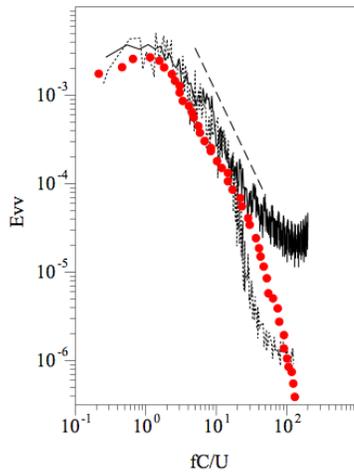
(b)
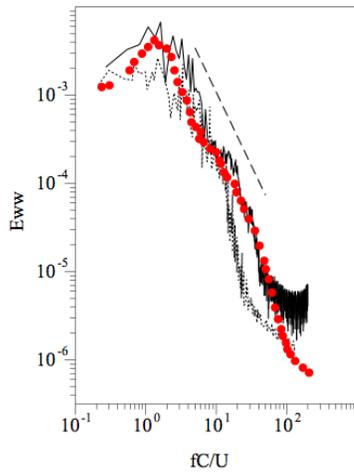
(c)

Figure 12: Energy spectra as a function of frequency in the tip-leakage region at $x/Ca = 1.51$, $y/Ca = 1.8$, $z/Ca = 0.1$. (a) E_{uu}; (b) E_{vv}; (c) E_{ww}. Solid lines are from the present LES, dotted lines are from coarse mesh LES,[6] symbols are from experiment[5], and dashed lines are of $-5/3$ slope.

(a)

(b)
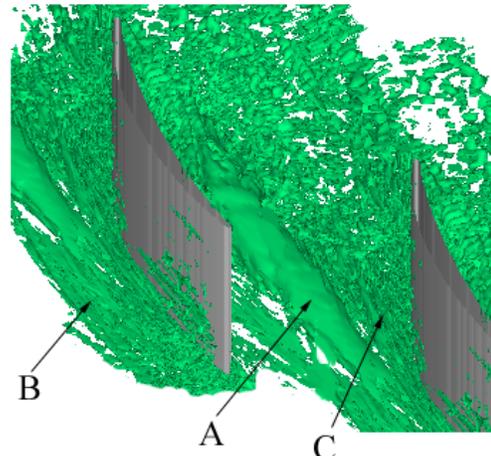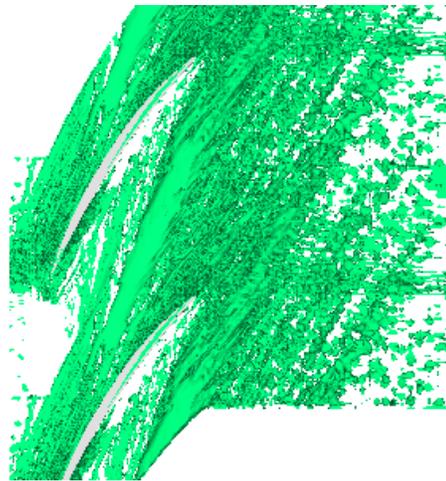
Figure 13: λ_2 iso-surfaces from time-averaged flowfield. (a) blade suction side view; (b) top view. A, B and C represent distinct vortical regions.
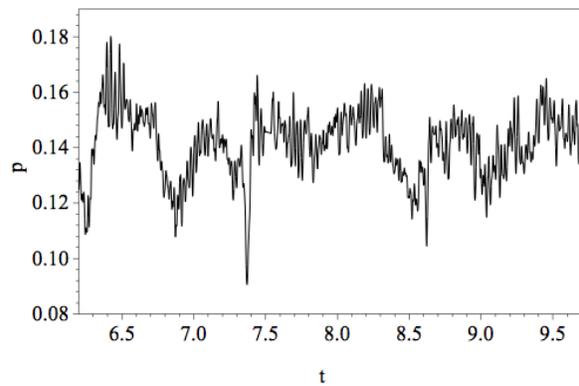
Figure 14: Temporal variation of pressure in the tip-leakage region at $x/Ca = 1.51$, $y/Ca = 1.8$, $z/Ca = 0.1$.
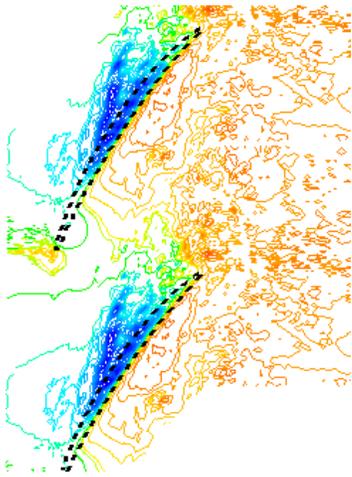
(a)
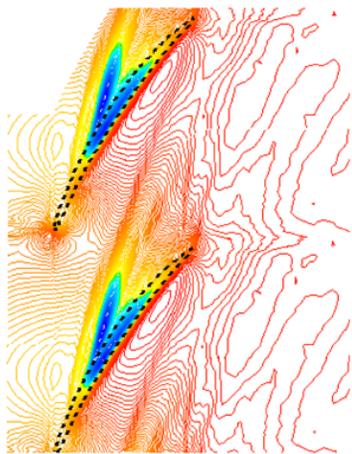
(b)
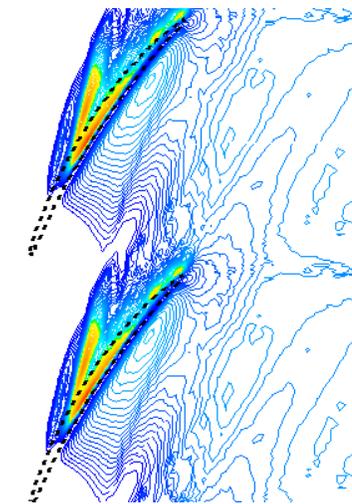
(c)

Figure 15: (a) Instantaneous, (b) time-averaged and (c) root mean squared pressure contours in an $x - y$ plane at $z/Ca = 0.0018$. Contour levels are from -0.25 to 0.25 by 0.01 for instantaneous and time-averaged pressure, and from 0.0003 to 0.01 by 0.0005 for root-mean squared pressure.
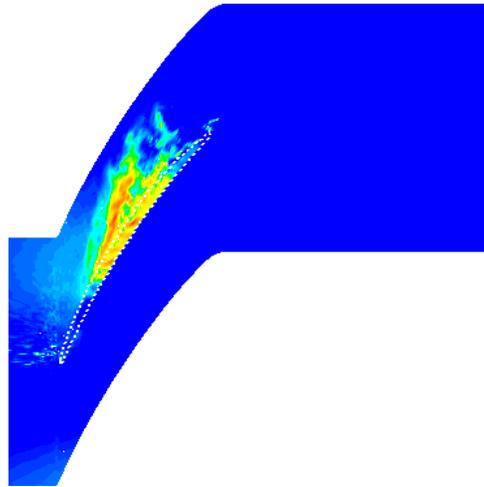
(a)
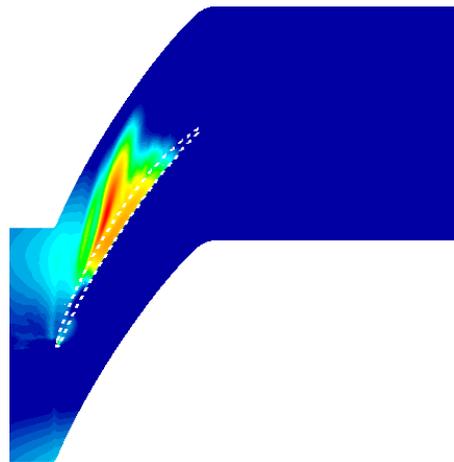
(b)

Figure 16: (a) Instantaneous and (b) time-averaged cavitation criterion, $B = 1/3(B_{11} + B_{22} + B_{33})$, contours in an x-y plane at $z/Ca = 0.0018$. Contour levels are from 0.030 to 0.30 by 0.05.

American Institute of Aeronautics and Astronautics